Electronic Supporting Information (ESI)

Pd Nanoparticles Deposited on $Co(OH)_2$ Nanoplatelets as a Bifunctional Electrocatalyst and their Application in Zn-air and Li-O_2 Batteries

*Suyeon Hyun [a], Apichat Saejio [b] and Sangaraju Shanmugam [a]**

[a] Department of Energy Science & Engineering,
Daegu Gyeongbuk Institute of Science & Technology (DGIST),
Daegu 42988, Republic of Korea
[b] Faculty of Engineering and Technology,
King Mongkut's University of Technology North Bangkok (KMUTNB),
Bankhai, Rayong, 21120, Thailand

*E-mail: sangarajus@dgist.ac.kr

Experimental

Material structure and physical properties characterization:

The phase of the catalysts was determined by X-ray diffraction (XRD, Rigaku, Miniflex 600). The Raman spectra were obtained with an excitation wavelength of 532 nm (Thermo Scientific, Nicolet Almega XR). The morphology of the catalysts and the air electrodes before and after battery cycling was characterized by field-emission scanning electron microscopy (FE-SEM, Hitachi, S-4800II, 3 kV) and a ultra-high resolution transmission electron microscope (Thermo Fisher Scientific, Themis Z). The XPS instrument (Thermo-Scientific/ESCALAB 250Xi) with Mg being the exciting source was operated to confirm the oxidation state of the catalysts. The elemental analysis was carried out to quantify the amount of carbon in the different catalysts (Vario MICRI cube).

Electrochemical characterization analysis:

The Koutecky-Levich plots were used to determine the ORR slope by the following equation.

$$\frac{1}{J} = \frac{1}{J_L} + \frac{1}{J_K} = \frac{1}{B\omega^{\frac{1}{2}}} + \frac{1}{J_K}$$

$$B = 0.62\, n\, F\, C_0\, D_0^{\frac{2}{3}}\, \nu^{-\frac{1}{6}}$$

Where, J_L is the diffusion-limiting current; J is the experimentally measured current; J_K is the kinetic current, F is the Faraday constant; ω is the angular velocity; C_0 is the saturated concentration of O_2 in 1 M KOH (1.2×10^{-6} mol cm^{-3}), D_0 is the diffusion coefficient of O_2 in 1 M KOH (1.9×10^{-5} cm^2 s^{-1}), and ν is the kinematic viscosity of the electrolyte. "n" can be calculated from the slope by under plot of J^{-1} vs. $\omega^{-1/2}$ and J_k is calculated from inverse of intercept. The OER measurement also carried out in 1 M KOH aqueous solution.

Table S1. Comparison of the OER catalytic activities of developed 1-Pd/$Co(OH)_2$ electrocatalysts with other reported non-precious metal based OER electrocatalysts in alkaline electrolyte.

Catalysts	Electrolyte	Overpotential (η) at 10 $mAcm^{-2}$	Reference
1-Pd/$Co(OH)_2$	1M KOH	390	This work
CoNi-LDH NSs	1M KOH	406	[1]
Co@Co_3O_4/NC	1M KOH	420	[2]
CoZn-NC-700	1M KOH	390	[3]
Au/$Co(OH)_2$	0.1M NaOH	320	[4]
Pd@PdO@Co_3O_4	0.1M KOH	310	[5]
Co@N-CNTF	1M KOH	400	[6]
CoS_2/N,S-GO	1M KOH	380	[7]

Table S2. Comparison of the ORR catalytic activities of developed 1-Pd/$Co(OH)_2$ electrocatalysts with other reported non-precious metal-based ORR electrocatalysts in alkaline electrolyte in 0.1 M KOH.

Catalysts	Onset potential (V vs. RHE)	Half-wave potential (V)	Limiting current density ($mAcm^{-2}$)	Ref.
1-Pd/$Co(OH)_2$	0.99	**0.87**	4.0	This work
$Co(OH)_2$/CoPt/N-CN	0.94	0.83	≈6.0	[8]
Au/$Co(OH)_2$	≈0.80	0.69	6.0	[4]
MWCNT/HL2-Pd(II)	0.95	≈0.85	5.0	[9]
CoZn-NC-700	0.98	0.84	4.93	[3]
NCNT/CoAl-LDH	0.925	0.812	5.45	[10]
Co@N-CNTF	0.91	0.81	≈5.0	[6]
Co@Co_3O_4/NC	0.90	0.80	4.5	[2]
Co-PDA-C	≈0.85	0.77	≈3.5	[11]
FeCo/N-DNC	0.89	0.81	6.0	[12]

Table S3. Summary of the primary Zn-air batteries with several key parameters for recently reported non-precious metal-based catalysts as an air electrode.

Air electrode catalyst	Anodic electrode	OCV (V)	Specific capacity ($mAhg^{-1}$)	Reference
1-Pd/Co(OH)$_2$	Zn foil	1.40	766 (5 $mAcm^{-2}$)	This work
CoN/NiO NWs	Zn foil	1.46	690 (5 $mAcm^{-2}$)	[13]
HP-Fe-N/CNFs	Zn foil	N.A.	701 (5 $mAcm^{-2}$)	[14]
N,P-CGHNs	Zn foil	1.50	712 (5 $mAcm^{-2}$)	[15]
Ni_3Fe/N-C	Zn foil	N.A.	528 (10$mAcm^{-2}$)	[16]
NGM-CN-Fe	Zn foil	1.40	654 (10$mAcm^{-2}$)	[17]
CoNi/BCF	Zn foil	1.44	711 (10$mAcm^{-2}$)	[18]

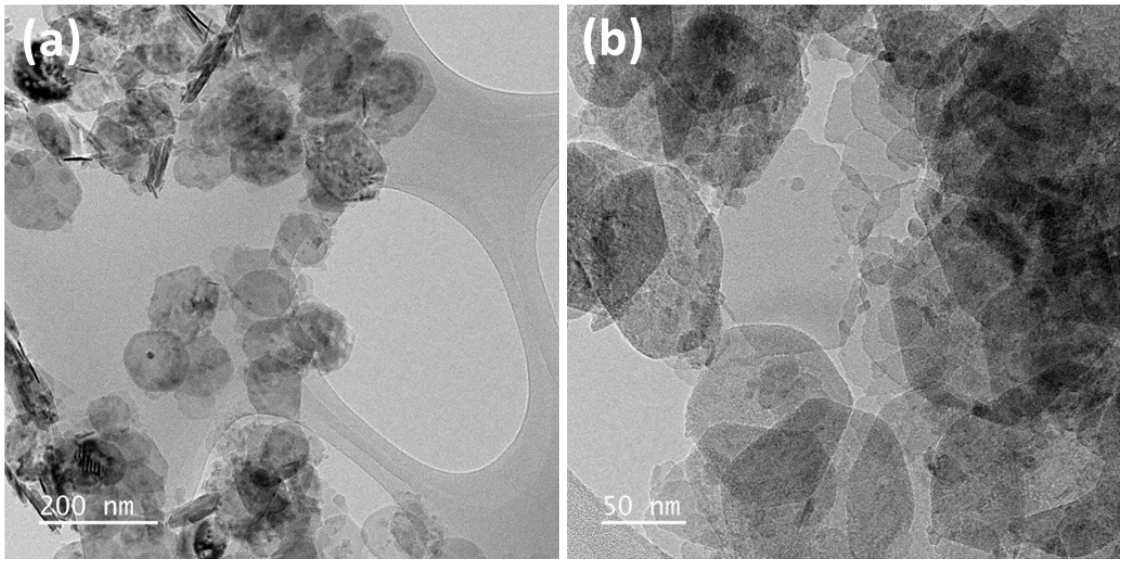

Fig. S1 Morphological characterization of catalysts: FE-TEM images of 2-Pd/$Co(OH)_2$.

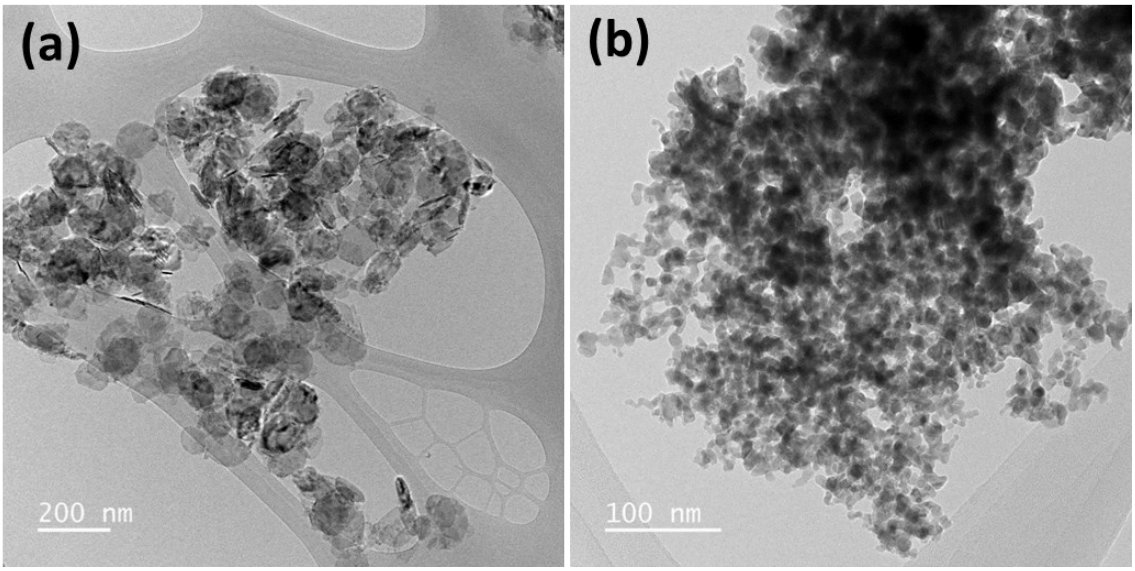

Fig. S2 Morphological characterization of catalysts: FE-TEM images of (a) $Co(OH)_2$ and (b) Pd.

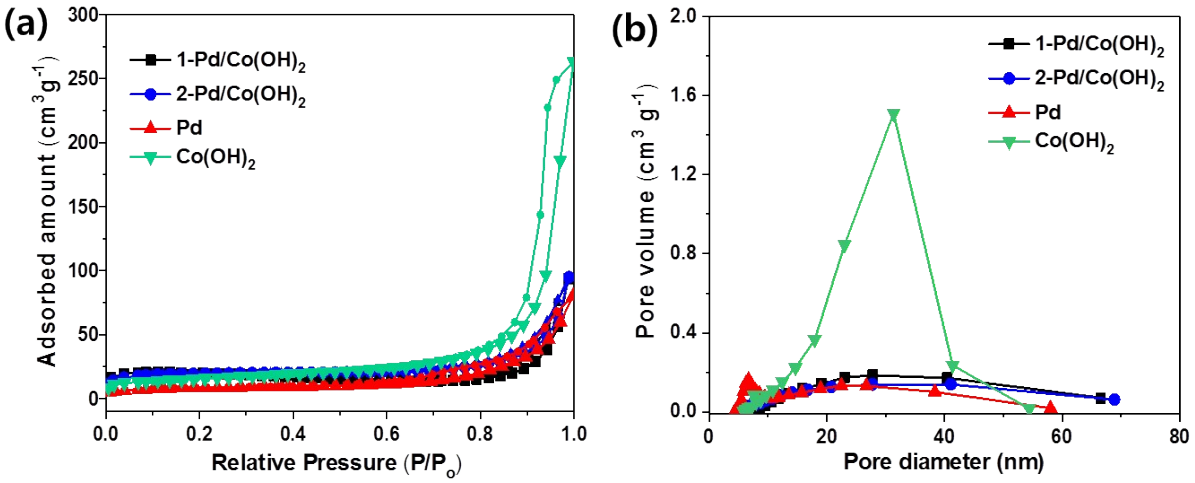

Fig. S3 BET surface area analysis: (a) N_2 adsorption–desorption isotherms and (b) pore diameter of all catalysts.

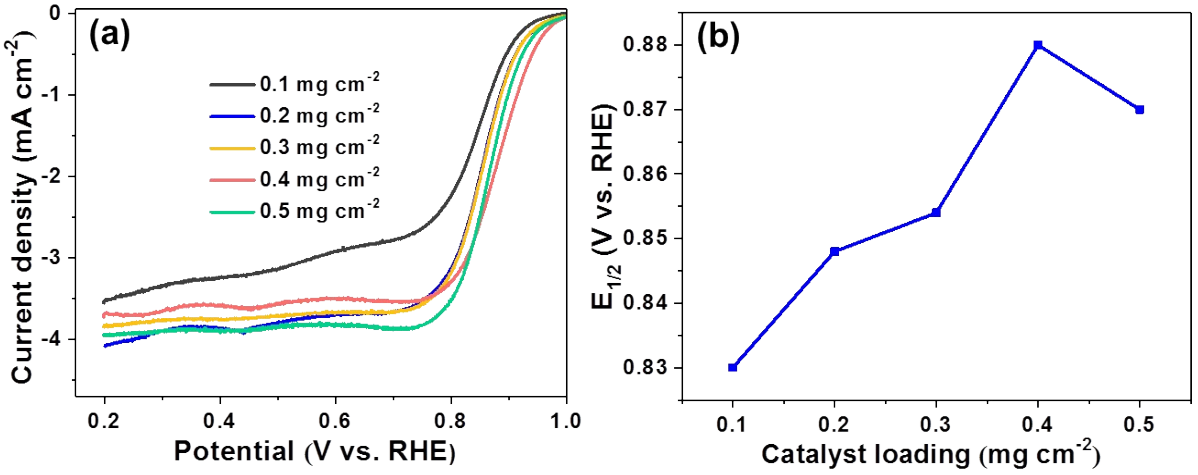

Fig. S4 ORR activities of 1-Pd/Co(OH)$_2$ catalyst. (a) LSV curves, (b) Half-wave potential ($E_{1/2}$) value corresponding to the various catalyst loading.

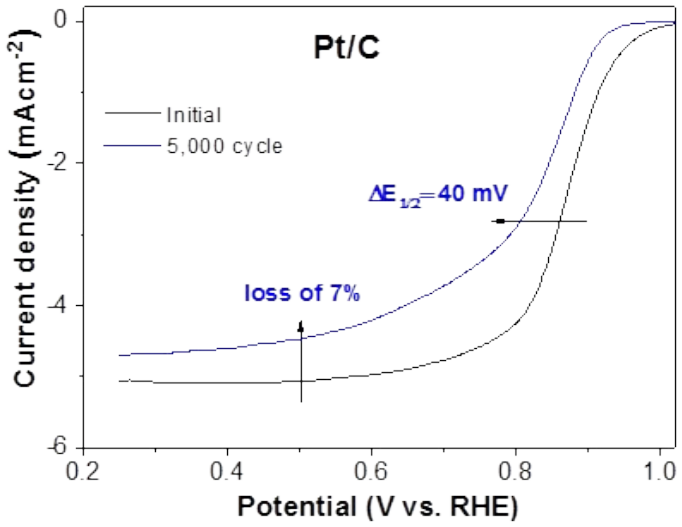

Fig. S5 ORR AST cycling test: LSV curves of Pt/C (20 wt%) during cycling stability test which is evaluated in a range of 0.6 to 1.0 V vs. RHE with a scan rate of 50 mVs^{-1}.

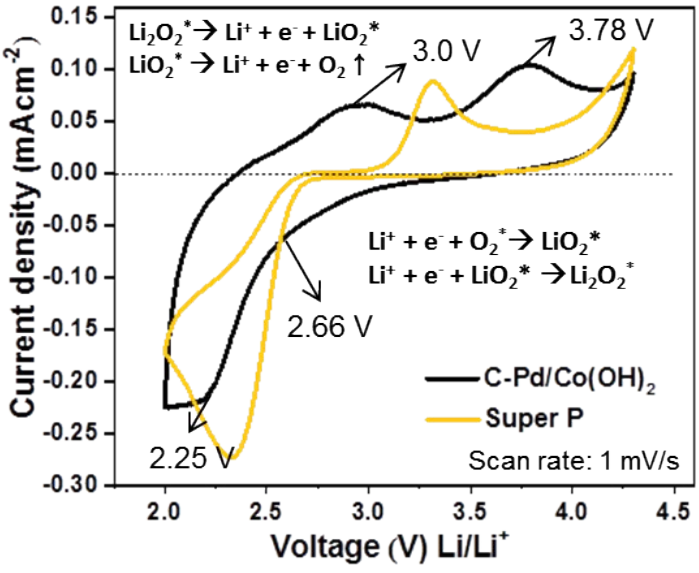

Fig. S6 CV curve of 1-Pd/$Co(OH)_2$ at a scan rate of 5 mV s^{-1} between 2.0 and 4.3 V.

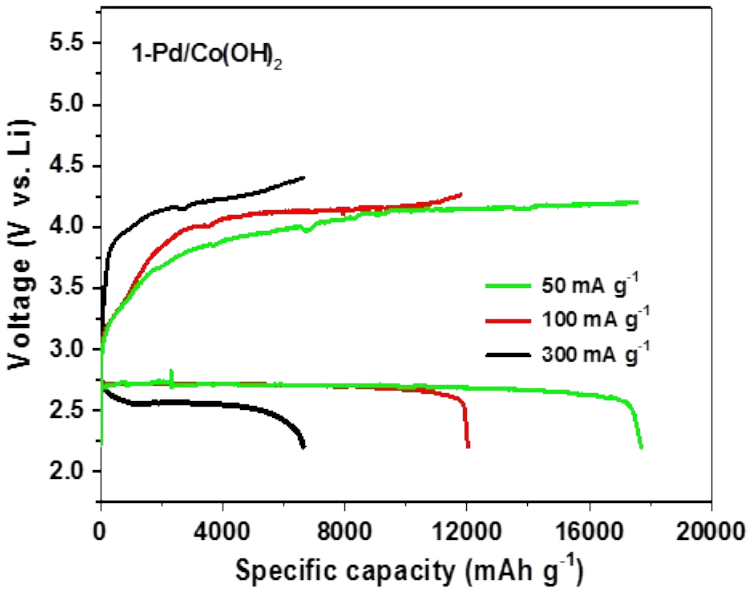

Fig. S7 The rate capability of Li-O_2 batteries based on 1-Pd/$Co(OH)_2$ electrode at various current densities.

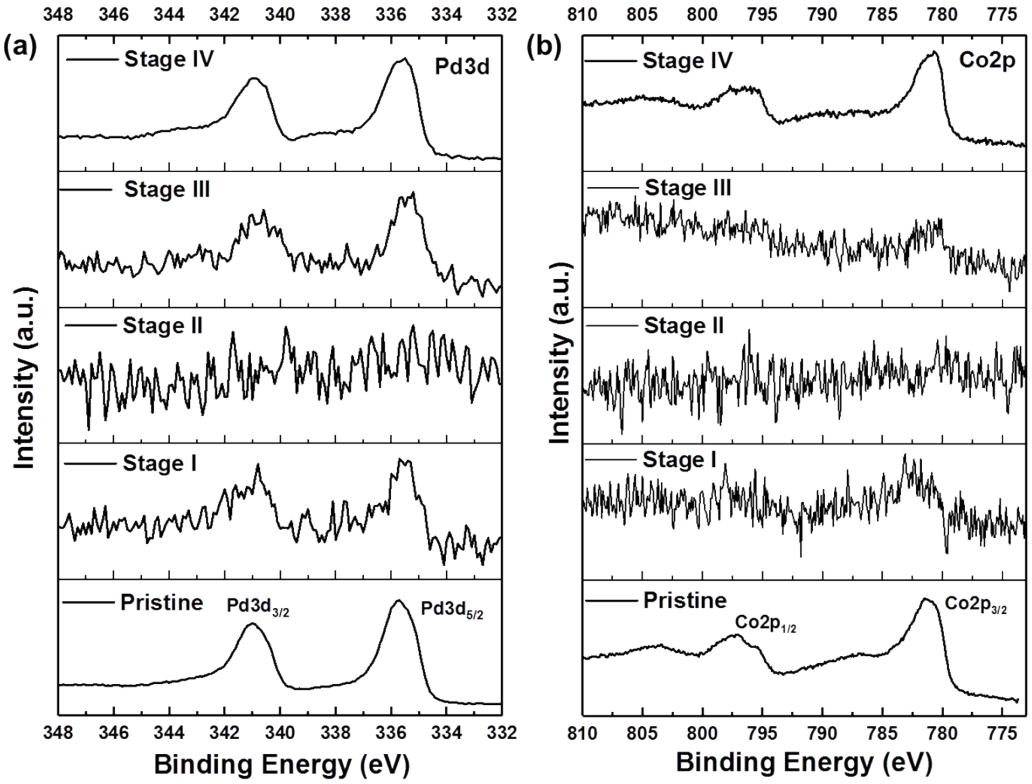

Fig. S8 XPS profiles of the 1-Pd/$Co(OH)_2$ cathode for (a) Pd3d and (b) Co2p at different stages in the discharge and charge process.

References

1. S. Yoon, J.-Y. Yun, J.-H. Lim and B. Yoo, *Journal of Alloys and Compounds*, 2017, **693**, 964-969.
2. A. Aijaz, J. Masa, C. Rösler, W. Xia, P. Weide, A. J. Botz, R. A. Fischer, W. Schuhmann and M. Muhler, *Angewandte Chemie International Edition*, 2016, **55**, 4087-4091.
3. B. Chen, X. He, F. Yin, H. Wang, D. J. Liu, R. Shi, J. Chen and H. Yin, *Advanced Functional Materials*, 2017, **27**, 1700795.
4. M. A. Sayeed and A. P. O'Mullane, *Journal of Materials Chemistry A*, 2017, **5**, 23776-23784.
5. H. C. Li, Y. J. Zhang, X. Hu, W. J. Liu, J. J. Chen and H. Q. Yu, *Advanced Energy Materials*, 2018, **8**, 1702734.
6. H. Guo, Q. Feng, J. Zhu, J. Xu, Q. Li, S. Liu, K. Xu, C. Zhang and T. Liu, *Journal of Materials Chemistry A*, 2019, **7**, 3664-3672.
7. Z. Jiang, Z.-J. Jiang, T. Maiyalagan and A. Manthiram, *Journal of Materials Chemistry A*, 2016, **4**, 5877-5889.
8. K. Wang, W. Wu, Z. Tang, L. Li, S. Chen and N. M. Bedford, *ACS Applied Materials & Interfaces*, 2019, **11**, 4983-4994.
9. M. Passaponti, M. Savastano, M. P. Clares, M. Inclán, A. Lavacchi, A. Bianchi, E. García-España and M. Innocenti, *Inorganic Chemistry*, 2018, **57**, 14484-14488.
10. W. Yu, H. Hou, Z. Xin, S. Niu, Y. Xie, X. Ji and L. Shao, *RSC Advances*, 2017, **7**, 15309-15314.
11. B. Li, Y. Chen, X. Ge, J. Chai, X. Zhang, T. A. Hor, G. Du, Z. Liu, H. Zhang and Y. Zong, *Nanoscale*, 2016, **8**, 5067-5075.
12. G. Fu, Y. Liu, Y. Chen, Y. Tang, J. B. Goodenough and J.-M. Lee, *Nanoscale*, 2018, **10**, 19937-19944.
13. J. Yin, Y. Li, F. Lv, Q. Fan, Y.-Q. Zhao, Q. Zhang, W. Wang, F. Cheng, P. Xi and S. Guo, *ACS Nano*, 2017, **11**, 2275-2283.
14. Y. Zhao, Q. Lai, Y. Wang, J. Zhu and Y. Liang, *ACS Applied Materials & Interfaces*, 2017, **9**, 16178-16186.
15. J. Yang, H. Sun, H. Liang, H. Ji, L. Song, C. Gao and H. Xu, *Advanced Materials*, 2016, **28**, 4606-4613.
16. G. Fu, Z. Cui, Y. Chen, Y. Li, Y. Tang and J. B. Goodenough, *Advanced Energy Materials*, 2017, **7**, 1601172.
17. C. Wang, H. Zhao, J. Wang, Z. Zhao, M. Cheng, X. Duan, Q. Zhang, J. Wang and J. Wang, *Journal of Materials Chemistry A*, 2019, **7**, 1451-1458.
18. W. Wan, X. Liu, H. Li, X. Peng, D. Xi and J. Luo, *Applied Catalysis B: Environmental*, 2019, **240**, 193-200.